Granular dynamics of density profiles in a suspension interface

C. Völtz*
Experimentalphysik V, Universität Bayreuth, D-95440 Bayreuth, Germany
(Received 22 January 2003; revised manuscript received 10 April 2003; published 26 August 2003)

The temporal evolution of the density profiles at the interface of a Rayleigh-Taylor instability in a sedimenting suspension is experimentally investigated. It is found that the sand-glycerin density gradients within the interface change with time, and that the evolution of the gradients differs significantly, depending on the location: The density profiles become steeper in the regions where the suspension flows downwards, whereas the profiles become flatter in the regions where the fluid flows upwards. This observation shows that there is a motion of the sand grains relative to the carrier fluid and hence reveals the prevailing granular dynamics in the suspension interface. It shows a behavior of the suspension which is different from the behavior of a homogeneous Newtonian one-component fluid whose density profiles do not change in time. Another interesting result is that the slopes of the profiles differ already at the very beginning ($t=0$) of the evolution of the instability, indicating that the suspension might have self-structured prior to instability onset.

DOI: 10.1103/PhysRevE.68.021408 PACS number(s): 83.80.Hj, 47.54.+r, 47.20.Ma

I. INTRODUCTION

In nature, the sedimentation of granular grains in a fluid is a familiar phenomenon with obvious importance in a wide range of industrial applications [1–3]. Hence suspensions have been studied for many years. Of special interest is the question, under which conditions a sedimenting suspension can be described as a Newtonian fluid, and under which conditions the granular properties of a suspension prevail (for a recent review see, e.g., Ref. [4]). In recent investigations of a suspension of high [5] and low [6] packing fraction under the influence of the Rayleigh-Taylor instability [7,8], the behavior of the suspensions was successfully compared with linear stability analyses for homogeneous Newtonian one-component fluids with vertically varying density and viscosity, where the models assume that the particle concentration in the flowing mixtures as well as the density profiles are constant (one-fluid model). The comparisons with the linear stability analyses for Newtonian fluids [5,6] provided a sufficient description of suspensions as homogeneous Newtonian fluids. However, in this paper we investigate the temporal evolution of the density profiles at the interface between the suspension and the pure fluid during the evolution of the Rayleigh-Taylor instability at distinct locations. This investigation shows that there is a motion of the grains relative to the carrier fluid, resulting in a temporal change in the steepness of the density gradients, which transcends the description of a suspension as a homogeneous one-component Newtonian fluid and gives a different facet to the description of suspension interfaces.

The paper is organized as follows: In the following section the experimental setup is described and in Sec. III the experimental results are discussed. A final section contains the conclusions.

*Present address: Laboratory of Atomic and Solid State Physics, Cornell University, Ithaca, New York 14853, USA. Email address: cv44@cornell.edu

II. EXPERIMENTAL SETUP

In order to establish the Rayleigh-Taylor instability in the suspension, a Hele-Shaw cell is turned upside down by means of a stepper motor in the same way as described in detail in Ref. [6].

The interfacial instability develops from a fairly sharp, flat interface between regions of different packing densities. To prepare the initial situation the self-sharpening effect of hindered settling is exploited [9]. Thus a sharp interface between the pure fluid and the sedimenting particles *below* the pure fluid is built. Then the vessel is rotated and the interface, now with glycerin and sand *above* pure glycerin, destabilizes, forming downward flowing suspension fingers and upward flowing pure fluid plumes.

For the experiments a closed Hele-Shaw cell with a width of 2 mm, a length of 98.0 mm, and a height of 50 mm (see Fig. 1) is filled with technical glycerin ($\sim$82%) as a carrier fluid and 2.0 g ''sand''. As sand we use spherical glass particles (Würth Ballotini MGL) with a material density of 2.45 g/cm^3 and a mean diameter of (61.13 ± 18.71) μm.

The temperature during all the measurements was stabilized to $25.32\,^{\circ}\mathrm{C}\pm0.01\,^{\circ}\mathrm{C}$. The standard deviation for any set of 201 measurements (see later) varies between $\pm0.004\,^{\circ}\mathrm{C}$ and $\pm0.008\,^{\circ}\mathrm{C}$. The material density of the technical glycerin was determined with a density balance to be 1.25 g/cm^3 at these temperatures.

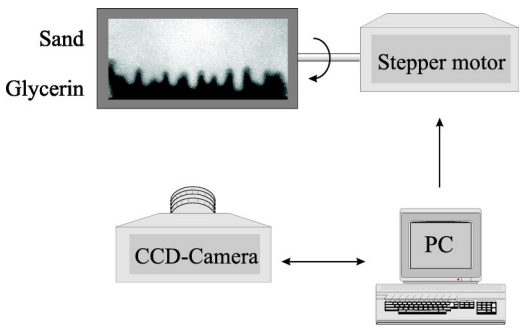

FIG. 1. Experimental setup; details in the text.

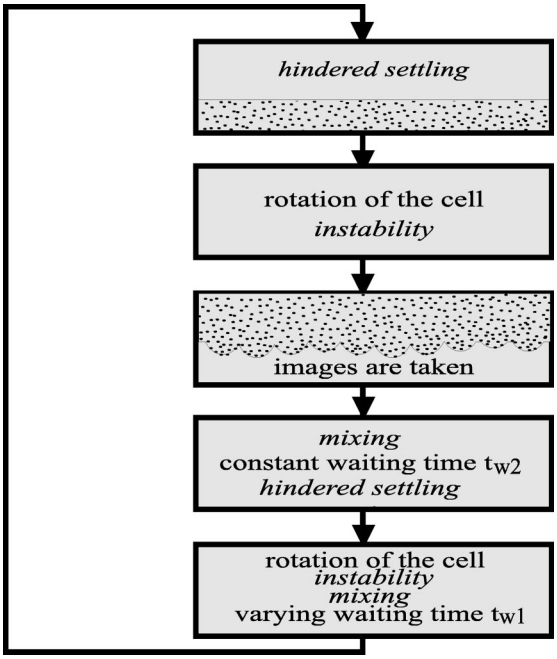

FIG. 2. Schematic procedure of the experimental cycle. By the different fonts the experimental preparation (normal font) and the system response (cursive font) are discriminated.

The cell is illuminated from behind by a field of light-emitting diodes which are run by dc current. The sand then appears bright in front of a dark background and can easily be detected by a charge-coupled device (CCD) camera connected to a frame grabber in the computer. The images have a dimension of 512×350 pixels. The optical resolution is given by $\Delta x=0.159$ mm/pixel. After an appropriate calibration between the gray scale and the packing density we obtain the packing fraction from the contrast of the pictures, which yields the local density of the suspension. For further details of the experimental setup see Ref. [6].

To prepare the initial interface the cell is revolved twice by the use of a stepper motor. At the very beginning the sand is lying at the bottom of the cell. Then the cell is revolved in 233 ms so that the sand is layered above the glycerin. This is the starting point of continuously repeating cycles (201 times). The sand sediments to the bottom of the cell and the self-sharpening effect forms a fairly sharp interface between the sedimenting suspension and the glycerin above. Before the sand has completed the sedimentation, the cell is revolved again after a varying waiting time t_{w1}, so that the suspension comes to lie above the glycerin. The instability of the interface between the suspension and the glycerin is observed. The camera starts to take 55 snapshots, 545 μs after the cell is turned. The time of the first snapshot defines the starting time $t=0$. The images are taken every second and show the middle part of the cell. After the images have been taken the cell is kept in its position for a constant waiting time $t_{w2}=5$ minutes. Then the cell is rotated again and the cycle repeats. Figure 2 shows schematically the various stages of the experimental cycle.

We have been able to prepare well defined distances of the interface from the horizontal walls by keeping $t_{w2}=5$ minutes constant and varying t_{w1} in seven sets (each of 201 measurements) with $t_{w1}=6,8,10,12,14,16,20$ min. The interface instability becomes active twice in every cycle. Apparently an effective mixing of the sand and the glycerin takes place, where memory effects are wiped out. In fact we observe that the interfaces at constant t_{w1} always form at the same height over the bottom of the cell. The averaged height h_{av} for every measurement is calculated by averaging the height of the interface in the lateral extension at $t=0$ s. Obviously the averaged height h_{av} increases monotonically with increasing t_{w1}. Figure 3 shows the dependence of the prepared height h_{av} as averaged over the 200 measurements on the varying waiting time t_{w1} (the first measurement of each series is not taken into account).

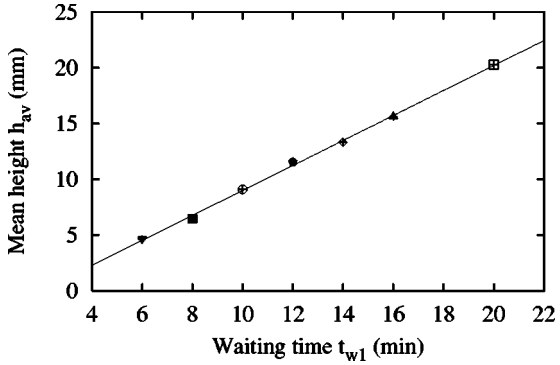

FIG. 3. Averaged height h_{av} as a function of t_{w1}. The different symbols represent the different waiting times t_{w1}: 20 min (open square), 16 min (filled triangle), 14 min (open rhombus), 12 min (filled pentagon), 10 min (open circle), 8 min (filled square), and 6 min (open triangle, upside down). The error bars, which cannot be resolved in this plot, give the standard deviation of the mean value.

As described, we obtain the packing fraction ϕ, which yields the local density of the suspension, from the contrast of the pictures. The density profiles $\phi(z)$ for the seven series of measurements are shown in Fig. 4, where z is the height of the cell in the vertical direction (antiparallel to gravity). The density profiles in Fig. 4 were smoothed with a cubic spline algorithm.

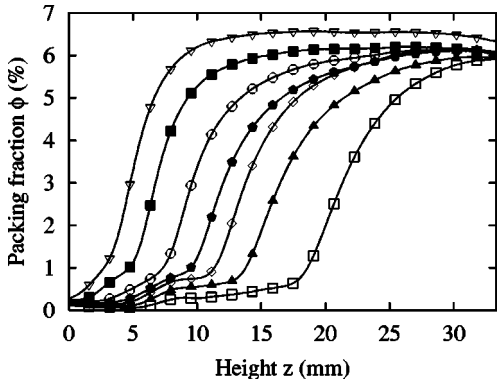

FIG. 4. Density profiles of different measurements, i.e., different t_{w1}. The profiles show different steepness and different distances to the vertical walls. The symbols are the same as in Fig. 3, Fig. 9, and Fig. 11 and are shown for every tenth data point.

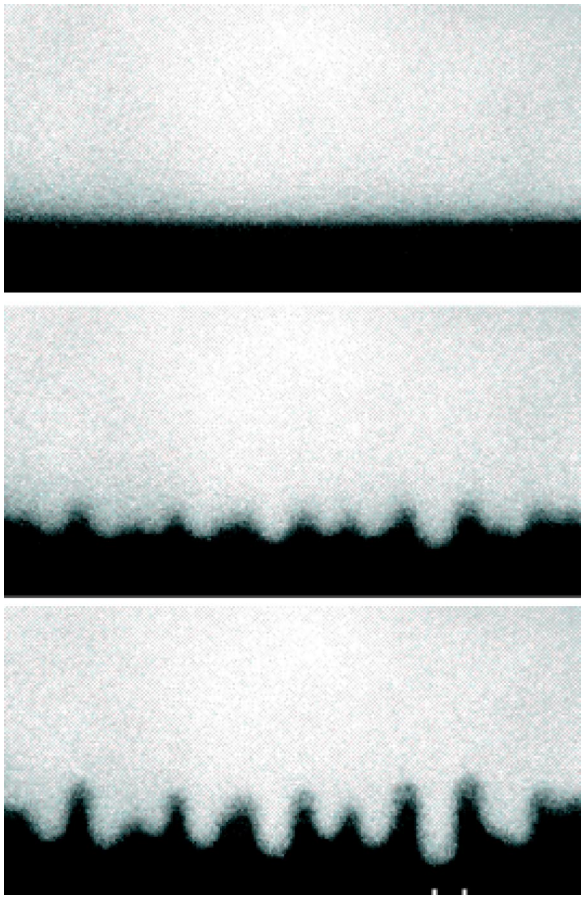

FIG. 5. Temporal evolution of the sand-glycerin interface at certain time steps: 0 s, 35 s, and 40 s. The frames show the middle part of the cell and have a horizontal length of 461 pixels, eqivalently, 73.3 mm. The bright color represents the sand-glycerin suspension, the dark color represents the glycerin. The contrast of the images is enhanced. Further details in the text.

III. EXPERIMENTAL RESULTS

The temporal evolution of the sand-glycerin interface at certain time steps is presented in Fig. 5. With the evolution of the interface, the density profiles $\phi(z)$ change dramatically. In this paper the temporal evolution of these density profiles is investigated at distinct positions in the interface, namely, at the positions where the longest suspension fingers flow downwards and at the positions where the highest glycerin plumes flow upwards.

After having acquired the digital images, these images are processed by an algorithm which finds the interface and also minimizes the mismatch between the left and right border of the interface by disregarding some (between 0 and 62) pixels at the edges in order to get rid of boundary effects at the side walls of the Hele-Shaw cell. (The algorithm is described in more detail in Ref. [6].) Figure 5 shows an example of the images without the pixels at the edges. At the point in time when the lowest part of the longest suspension finger has reached half the height between its initial height and the bottom of the cell, the spanwise horizontal x coordinates of the lowest point of the longest suspension finger and of the highest point of the highest glycerin plume are specified and

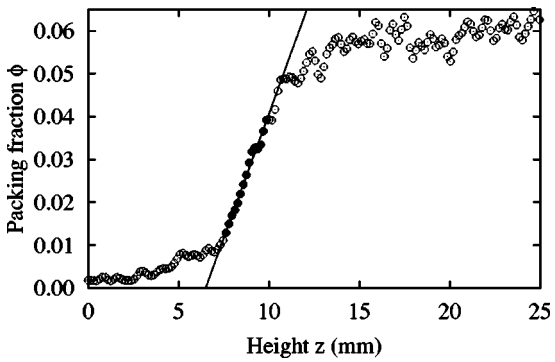

FIG. 6. Linear fit to the profile at $t=0$ at the x coordinate, where the suspension will flow downwards later. The open symbols represent the profile, while the filled symbols represent the data for the fit. The data belong to a measurement of the series with $h_{av}=9.1$ mm.

the z profiles for these pixels are obtained. In Fig. 5 the x coordinate for the lowest point of the longest suspension finger and of the highest point of the highest suspension plume are indicated by the white short lines at the bottom of the figure. The profiles in z direction at these pixel locations are then averaged with the neighboring two profiles for every point of time of every single measurement. A linear fit to these profiles is then obtained, which contains the first 15 data points with $\phi>0.012$. Figure 6 shows a fit to the profile at the time $t=0$ at the location, where the suspension will flow downwards at later points in time.

The 200 measurements per series give 200 gradients at 55 times. These gradients of the line fits are averaged over these 200 measurements of every series to obtain a mean gradient for the locations where the suspension fingers flow downwards and for the locations where the glycerin plumes flow upwards for every time step. Figure 7 shows the temporal evolution of this mean concentration gradient. The density gradients for both regions are almost the same at the beginning of the instability, but they change clearly during the evolution of the instability: The concentration gradient in-

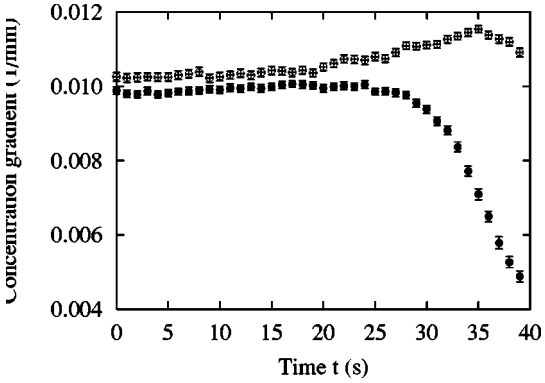

FIG. 7. Temporal evolution of the concentration gradient in the region where the suspension flows downwards (open symbols) and in the region where the glycerin flows upwards (filled symbols). The data show the mean value of 200 single measurements, the error bars give the standard deviation of the mean value. The data belong to a measurement of the series with $h_{av}=9.1$ mm.

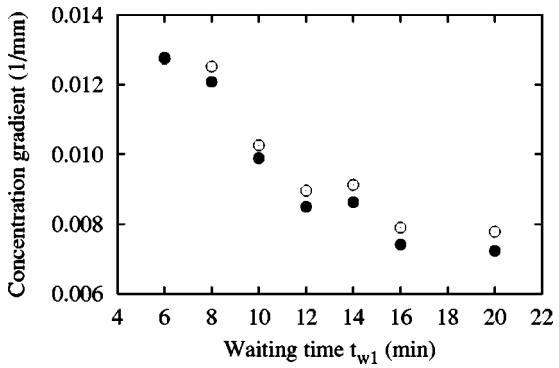

FIG. 8. Concentration gradient over t_{w1} at $t=0$ in the region where the suspension flows downwards (open symbols) and in the region where the glycerin flows upwards (filled symbols). For $t_{w1}=6$ min the symbols overlap.

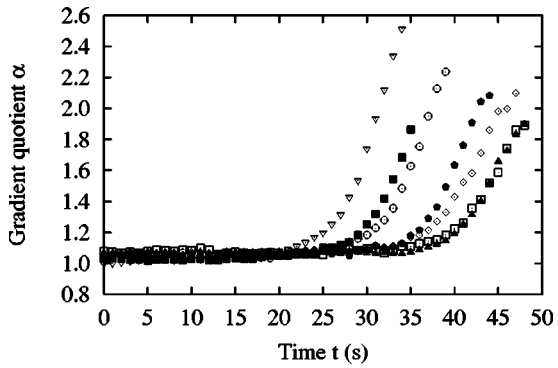

FIG. 9. Temporal evolution of the gradient quotient α for all series of measurements. The symbols are the same as in Fig. 3, Fig. 4, and Fig. 11.

creases with time at the location where the suspension flows downwards and decreases where the glycerin flows upwards. The fact that the gradients of the profiles change in time indicates that the sand rearranges within the layer of the interface. For every measurement the analysis is stopped at the time when the lowest point of the longest suspension finger has moved half the height between its initial position and the bottom boundary of the cell. For the measurement shown in Fig. 7 this is the case at $t=39$ s. At this time the longest finger is only 4.5 mm away from the bottom boundary of the cell. The distance of the upwards flowing glycerin plume to the upper boundary of the Hele-Shaw cell is always in the order of cm for all seven series of measurements. The boundary effect for the downwards flowing suspension fingers becomes apparent in the decrease of the concentration gradient for the downward flowing suspension for $t>35$ s in Fig. 7.

A possible explanation for the steepening of the profiles in the region of the suspension finger flowing downwards could be as follows: The fluid carries downwards more of the sand with higher packing density above the interface than of the sand with small packing density within the interface. This means that the profile becomes steeper over time. The scenario for the upward flowing glycerin plume would be analogous: In the region where the glycerin flows upwards it carries away more of the sand with higher packing density above the interface than of the sand with small packing density below. This means that the profile becomes less steep over time.

In Fig. 8 the concentration gradient is shown for all seven series at $t=0$. It is striking that already at this time there is a clear tendency that the gradient of the concentration profiles is higher at that position where afterwards the suspension will flow downwards than at the position where later the glycerin will flow upwards. Furthermore, it is obvious that the gradient of the density profiles decreases with the waiting time t_{w1}.

In order to analyze the temporal evolution of the rearrangement of the sand even further,

$$(\text{gradient quotient } \alpha) = \frac{(\text{gradient of downward flowing suspension})}{(\text{gradient of upward flowing glycerin})}$$

is determined. This quantity α is approximately 1 at the beginning of the instability process and increases with time. Figure 9 shows the temporal increase of α for all seven series. It is obvious that the gradient quotient α increases faster for the series with small h_{av} than for series with larger h_{av} (compare Fig. 3 with Fig. 9). The temporal increase of the gradient quotient α seems to be exponential, which suggests fitting an exponential growth law to the data. From an exponential fit to

$$\alpha(t)=\alpha_i \exp(\sigma_\alpha t)+\alpha_0, \tag{3.1}$$

the growth rate σ_α as well as α_0 and α_i are determined. The fit of the offset α_0, according to the empirically chosen Eq. (3.1) is a trick of the data analysis which allows us to draw a conclusion about the initial perturbation of the system.

Figure 10 shows the exponential fit to the gradient quotient for the series with $h_{av}=9.1$ mm according to Eq. (3.1). The value of $\alpha_0+\alpha_i$ at $t=0$ is shown in Fig. 11. The systematic increase of $\alpha_0+\alpha_i$ for increasing height over the bottom of the cell is striking. This means that for larger h_{av} and hence for larger waiting times t_{w1}, the initial quotient of the gradients at the different positions increase. This astonishing result can be interpreted in the way that the sand has more time for its rearrangement when t_{w1} is larger so that the self-structuring would then be more pronounced, provided

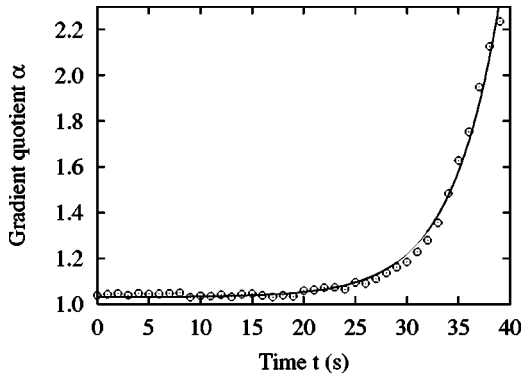

FIG. 10. Temporal evolution of the gradient quotient α and an exponential fit according to Eq. (3.1). The data belong to a measurement of the series with $h_{av}=9.1$ mm.

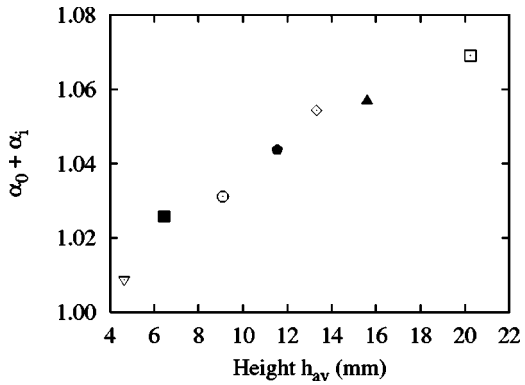

FIG. 11. Initial value $\alpha_0+\alpha_i$. The symbols are the same as in Fig. 3, Fig. 4, and Fig. 9.

that the self-structuring and hence the order within the sedimenting suspension increase with time. This structuring of the sand within the suspension could then determine the location where the suspension will flow downwards and the glycerin will flow upwards after the rotation of the cell.

Structure, density, and velocity fluctuations in non-Brownian suspensions have been reported in the literature [10]. To our knowledge a temporal increase of these fluctuations has not yet been analyzed. In bidisperse suspensions a tendency can be observed for particles of the same species to accumulate and induce a vertical flow [11]. It can be speculated that in our experiment the variance in the particle size has given rise to an effect of this kind and has induced vertical currents of small magnitude.

IV. CONCLUSIONS

In a closed Hele-Shaw cell the temporal evolution of the density profiles of the interface of a sedimenting suspension under the Rayleigh-Taylor instability was investigated. The evaluation provides insights in the dynamics of the sand grains within the interface during the development of the instability by showing that the density profiles are changing with time and that the evolution of the profiles depends on the location. The gradients become steeper in the regions where the suspension flows downwards whereas they are diluted in the regions where the glycerin flows upwards. The fact that the profiles change their steepness means that the suspension changes its local density and that there is a motion of the sand grains relative to the carrier fluid. Hence there is a granular dynamics within the suspension interface. This description of a suspension transcends the description of a suspension as a homogeneous one-component Newtonian fluid (one-fluid model), which was recently applied for describing the behavior of suspensions from a different viewpoint [5,6]. In this continuum approach the suspension is considered as a homogeneous fluid which should move as a continuous media, thereby not changing its density (and hence its packing fraction).

Furthermore, the sand does not only rearrange during the development of the instability but there are indications that prior to the rotation of the cell the suspension self-structures and that this structuring becomes stronger with the time of sedimentation. It can be speculated that these patterns might determine the locations of the upward and downward flowing currents after the rotation of the cell.

ACKNOWLEDGMENTS

It is a pleasure to thank Ingo Rehberg and Werner Pesch for many stimulating discussions. The experiment was supported by Deutsche Forschungsgemeinschaft through Grant No. Re588/12.

[1] M. Ungarish, *Hydrodynamics of suspensions* (Springer, New York, 1993).
[2] *Sedimentation of Small Particles in a Viscous Fluid*, edited by E.M. Tory (Computational Mechanics Publications, Southampton, 1996).
[3] H.A. Barnes, *Dispersion Rheology: 1980* (Royal Society of Chemistry, Industrial Division, London 1981).
[4] J. Gollub, Phys. Today **56**(1), 10 (2003).
[5] C. Völtz, M. Schröter, G. Iori, A. Betat, A. Lange, A. Engel, and I. Rehberg, Phys. Rep. **337**, 117 (2000).
[6] C. Völtz, W. Pesch, and I. Rehberg, Phys. Rev. E **65**, 011404 (2002).
[7] Lord Rayleigh, Scientific Papers, Vol. II (Cambridge University Press, Cambridge, England, 1900), p. 200.
[8] G.I. Taylor, Proc. R. Soc. London, Ser. A **201**, 192 (1950).
[9] G.J. Kynch, Trans. Faraday Soc. **48**, 166 (1952); R.H. Davis and A. Acrivos, Annu. Rev. Fluid Mech. **17**, 91 (1985); R.H. Davis and M.A. Hassen, J. Fluid Mech. **196**, 107 (1988).
[10] F. Rouyer, D. Lhuillier, J. Martin, and D. Salin, Phys. Fluids **12**, 958 (2000).
[11] G.K. Batchelor and R.W.J. van Rensburg, J. Fluid Mech. **166**, 379 (1986).